

Benchmark ab Initio Characterization of the Complex Potential Energy Surface of the $\text{Cl}^- + \text{CH}_3\text{I}$ Reaction

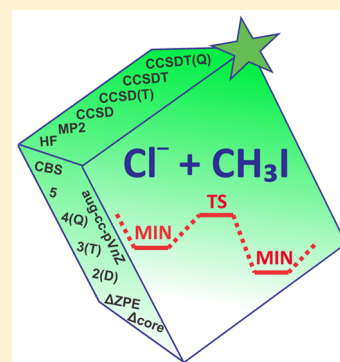
István Szabó[†] and Gábor Czakó^{*†}

Department of Physical Chemistry and Materials Science, Institute of Chemistry, University of Szeged, Rerrich Béla tér 1, Szeged H-6720, Hungary

Supporting Information

ABSTRACT: Benchmark stationary-point structures, vibrational frequencies, and classical/adiabatic relative energies (kcal/mol) are reported for the $\text{Cl}^- + \text{CH}_3\text{I}$ reaction along the back-side attack ($\Delta E_{\text{TS}} = -5.48/-5.54$) inversion, front-side attack ($\Delta E_{\text{TS}} = 36.73/35.89$) and double-inversion ($\Delta E_{\text{TS}} = 46.97/42.55$) retention $\text{S}_{\text{N}}2$ pathways, the proton-transfer channel, and the hydride-substitution reaction path. The structures and frequencies are obtained by the frozen-core CCSD(T), CCSD(T)-F12a, and CCSD(T)-F12b methods with the aug-cc-pVnZ [$n = \text{D, T, and Q}$ for structures and $n = \text{D and T}$ for frequencies] basis sets and all-electron CCSD(T) with aug-cc-pwCVnZ [$n = \text{D and T}$ for structures and $n = \text{D}$ for frequencies]. The benchmark relative energies are determined using the focal-point analysis approach based on electron correlation methods up to CCSDT(Q), extrapolations to the complete basis set limits using aug-cc-pVnZ [$n = 2(\text{D}), 3(\text{T}), 4(\text{Q}),$ and 5] bases, core correlation contributions obtained at CCSD(T)/aug-cc-pwCVQZ, and, for the adiabatic energies, zero-point energy corrections at the CCSD(T)-F12b/aug-cc-pVTZ level of theory.

We usually find significant method and modest basis dependence for the energies. The post-CCSD(T) and core correlation effects are often about 0.4 kcal/mol, but almost cancel each other. The explicitly correlated CCSD(T)-F12 methods are recommended for geometry and frequency computations as well as for energy computations if the basis set dependence is significant.



I. INTRODUCTION

Stationary points on the potential energy surface (PES) of a chemical system play a key role in the kinetics and dynamics studies of reactions. The reactants and products are usually separated by a first-order saddle point, called transition state (TS), whose structure and relative energy may control the outcome of a chemical reaction, at least at low collision energies. Whereas the direct experimental observation of these stationary points is very challenging, their accurate quantum chemical determination is feasible nowadays. The qualitative pictures of stationary points of the bimolecular nucleophilic substitution ($\text{S}_{\text{N}}2$) reactions can be found in every organic chemistry textbook, and many electronic structure studies were reported in the past couple of decades providing quantitative descriptions of the minima and TSs.^{1–5} The dogmatic approach of $\text{S}_{\text{N}}2$ reactions presumes a double-well potential featuring ion-dipole complexes in the entrance and product channels and a central TS separating the two minima. The reaction pathway going through these stationary points is called back-side attack Walden inversion, which is probably the best-known stereospecific reaction mechanism in chemistry. However, recent studies showed that the PES of the $\text{S}_{\text{N}}2$ reactions is much more complex.^{6–10} Besides the above-mentioned stationary points, hydrogen-bonded^{6,11,12} and front-side^{13,9,14} complexes can be formed, and retention mechanisms can occur via a front-side attack^{15–17,7–10} or a double-inversion^{7–9} TS. Front-side attack is less-known than the back-side attack inversion mechanism,

although the former was also described in the early book of Ingold.¹⁸ Double inversion (DI), in which a proton-abstraction-induced inversion is followed by a second inversion via a Walden-TS, was recently discovered by us by analyzing quasiclassical trajectories on an analytical PES of the $\text{F}^- + \text{CH}_3\text{Cl}$ reaction.⁷ Later we reported DI TSs for the $\text{X}^- + \text{CH}_3\text{Y}$ [$\text{X, Y} = \text{F, Cl, Br, I}$] reactions¹⁹ and found DI trajectories for $\text{F}^- + \text{CH}_3\text{F}$,⁸ $\text{F}^- + \text{CHD}_2\text{Cl}$,²⁰ and $\text{F}^- + \text{CH}_3\text{I}$.⁹ Very recently a direct dynamics study of Hase and co-workers also revealed DI pathways for $\text{F}^- + \text{CH}_3\text{I}$. Furthermore, Wang and co-workers identified the DI mechanism for $\text{F}^- + \text{CH}_3\text{Cl}$ and $\text{F}^- + \text{CH}_3\text{I}$ in aqueous solution.^{21,22} Moving toward larger systems, we can say that the DI TS was also found for the $\text{F}^- + \text{CH}_3\text{CH}_2\text{Cl}$ reaction.²³

Besides the $\text{S}_{\text{N}}2$ pathways of the above-mentioned ion-molecule reactions, the proton-abstraction (proton transfer from the molecule to the nucleophilic ion) is also an important reaction channel. Recent studies on the $\text{F}^- + \text{CH}_3\text{I}$ reaction of Hase and co-workers²⁴ revealed that not one or two, but several stationary points are involved in the proton-transfer process, which are all described by our recent analytical PES.⁹ Furthermore, the DI mechanism and the proton abstraction

Received: June 5, 2017

Revised: July 7, 2017

Published: July 10, 2017



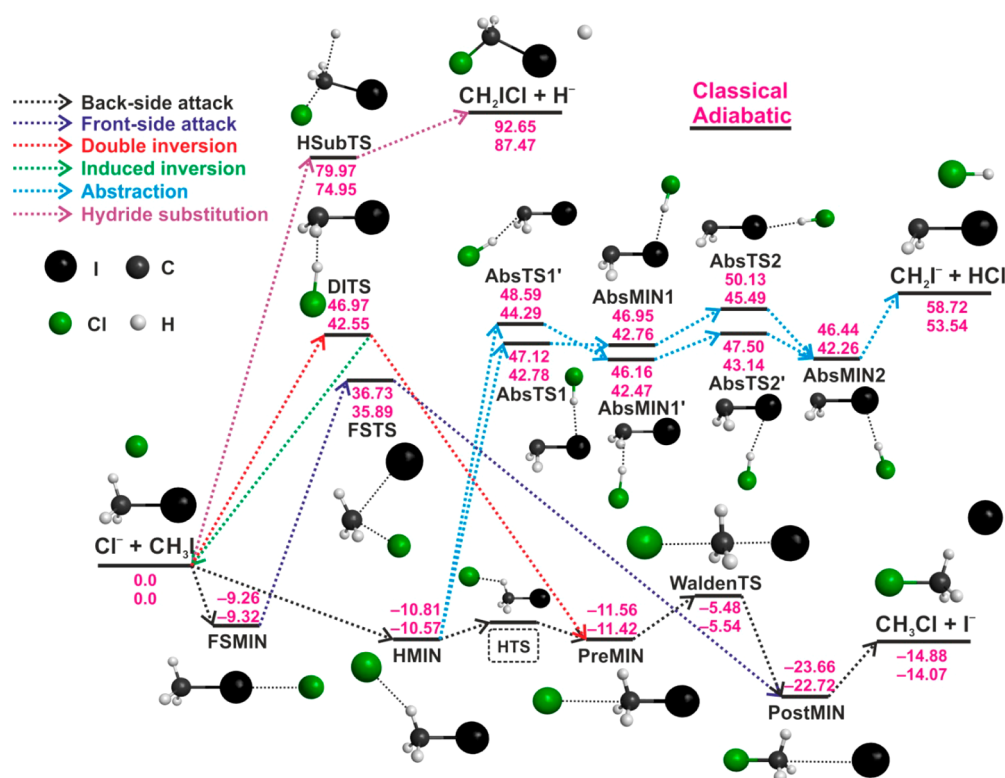


Figure 1. Potential energy diagram of the $\text{Cl}^- + \text{CH}_3\text{I}$ reaction showing the stationary points and their benchmark relative energies (kcal/mol) along the different reaction pathways. (Double inversion shown here may not be an IRC pathway.) The high-level classical relative energies are obtained from the focal-point analysis approach as $\text{CCSD(T)}/\text{CBS} + \delta[\text{CCSDT}] + \delta[\text{CCSDT(Q)}] + \Delta_{\text{core}}[\text{CCSD(T)}/\text{aug-cc-pwCVQZ}]$, and the adiabatic energies include $\Delta\text{ZPE}[\text{CCSD(T)-F12b}/\text{aug-cc-pVTZ}]$ as well.

are closely related because the first step of DI is a proton-abstraction induced inversion.

Based on the above-described findings now it is clear that the PES of an $\text{X}^- + \text{CH}_3\text{Y}$ reaction is quite complex, having a lot of important stationary points. Therefore, one may start rethinking $\text{S}_{\text{N}}2$ reactions like Xie and Hase did in their recent review.¹⁰ In the present study we focus on the $\text{Cl}^- + \text{CH}_3\text{I}$ reaction due to the following reasons: (a) detailed experimental differential cross sections and product internal energy distributions are available for the $\text{Cl}^- + \text{CH}_3\text{I}$ $\text{S}_{\text{N}}2$ reaction;^{25,26} in fact, this was the system for which Wester and co-workers reported their pioneering crossed-beam imaging experiment of $\text{S}_{\text{N}}2$ dynamics;²⁵ (b) direct dynamics simulations were performed and the computed results usually reproduce experiment; however, at a certain collision energy theory and experiment disagree motivating further investigation of the title reaction;²⁶ and (c) in 2009 Hase and co-workers²⁷ reported a detailed electronic structure study of the stationary points; however, only the pre- and postreaction ion–dipole complexes and the Walden TS were considered. Here, we plan to present a more complex picture of the title reaction considering hydrogen-bonded and front-side complexes, front-side attack and double-inversion retention pathways, many stationary points along the proton-transfer channel, and several additional high-energy product channels in addition to the well-known ion–dipole complexes and Walden-inversion TS. Besides the standard CCSD(T) method²⁸ we use the novel explicitly correlated CCSD(T)-F12 methods²⁹ to characterize all the above-mentioned stationary points. Furthermore, we will consider effects, such as core-electron and post- CCSD(T) correlation, which are usually neglected in electronic structure

studies of $\text{S}_{\text{N}}2$ reactions. Thus, we report benchmark relative energies of the stationary points of the $\text{Cl}^- + \text{CH}_3\text{I}$ reaction, which can be used as reference in future theoretical and experimental studies and guide others when investigating similar systems. In section II, the applied methods are described in detail, and in section III, the results are reported and discussed. The article ends with a summary and conclusions in section IV.

II. COMPUTATIONAL DETAILS

Structures of the minima and saddle points are computed by the standard coupled-cluster singles, doubles, and perturbative triples [CCSD(T)] method²⁸ as well as by the explicitly correlated CCSD(T)-F12a and CCSD(T)-F12b methods²⁹ using the correlation-consistent aug-cc-pVnZ [$n = 2(\text{D}), 3(\text{T}), 4(\text{Q})$] basis sets.³⁰ For iodine, a relativistic effective core potential, which replaces the inner core $1s^2 2s^2 2p^6 3s^2 3p^6 3d^{10}$ electrons, and the corresponding aug-cc-pVnZ-PP basis sets are employed.³¹ All of the above computations use the usual frozen-core approach correlating the valence electrons only. All-electron (AE) computations, correlating all the valence electrons and the $1s^2, 2s^2 2p^6,$ and $4s^2 4p^6 4d^{10}$ core electrons of C, Cl, and I, respectively, are also performed using CCSD(T) with the aug-cc-pwCVDZ and aug-cc-pwCVTZ basis sets³² (and the corresponding PP bases³³ for I). Harmonic vibrational frequencies are determined using the frozen-core $\text{CCSD(T)}, \text{CCSD(T)-F12a},$ and CCSD(T)-F12b methods with the aug-cc-pVnZ [$n = 2(\text{D})$ and $3(\text{T})$] basis sets and the all-electron CCSD(T) with aug-cc-pwCVDZ.

Benchmark relative energies of the stationary points are obtained by the focal-point analysis^{34,35} approach considering

Table 1. Benchmark Classical and Adiabatic Energies (kcal/mol) of the Stationary Points Relative to $\text{Cl}^- + \text{CH}_3\text{I}$ Obtained from the Focal-Point Analysis Approach^a

stac. point	CCSD(T)/CBS ^b	$\delta[\text{CCSDT}]^c$	$\delta[\text{CCSDT(Q)}]^c$	Δcore^d	classical ^e	ΔZPE^f	adiabatic ^g
HMIN	-10.74	-0.02	-0.03	-0.02	-10.81	+0.24	-10.57
PreMIN	-11.48	-0.03	-0.04	-0.01	-11.56	+0.15	-11.42
PostMIN	-24.12	+0.00	+0.02	+0.44	-23.66	+0.95	-22.72
FSMIN	-9.35	+0.00	-0.12	+0.21	-9.26	-0.06	-9.32
FSMIN'	-14.15	+0.02	+0.02	+0.53	-13.58	+0.85	-12.73
AbsMIN1	46.97	-0.14	-0.16	+0.28	46.95	-4.19	42.76
AbsMIN1'	46.06	-0.07	-0.22	+0.39	46.16	-3.69	42.47
AbsMIN2	46.48	-0.14	-0.17	+0.27	46.44	-4.18	42.26
WaldenTS	-5.50	-0.15	-0.20	+0.36	-5.48	-0.06	-5.54
FSTS	37.17	-0.31	-0.64	+0.51	36.73	-0.84	35.89
DITS	47.03	+0.03	-0.29	+0.21	46.97	-4.42	42.55
AbsTS1	47.12	-0.13	-0.15	+0.29	47.12	-4.34	42.78
AbsTS1'	48.35	-0.09	-0.17	+0.50	48.59	-4.30	44.29
AbsTS2	50.10	-0.15	-0.16	+0.34	50.13	-4.64	45.49
AbsTS2'	47.46	-0.12	-0.17	+0.34	47.50	-4.37	43.14
HSubTS	80.21	-0.17	-0.47	+0.40	79.97	-5.02	74.95
$\text{I}^- + \text{CH}_3\text{Cl}$	-15.56	+0.02	+0.05	+0.61	-14.88	+0.81	-14.07
$\text{HCl} + \text{CH}_2\text{I}^-$	58.36	-0.13	-0.11	+0.60	58.72	-5.18	53.54
$\text{H}^- + \text{CH}_2\text{ICl}$	92.74	+0.15	-0.10	-0.14	92.65	-5.19	87.47
$\text{I}^- \cdots \text{HCl} + \text{CH}_2^h$	76.85	-0.31	+0.05	+0.81	77.40	-7.65	69.75
$\text{ICl}^- + \text{CH}_3$	37.28	-0.12	+0.06	+0.79	38.00	-4.02	33.99
$\text{ICl} + \text{CH}_3^-$	92.75	-0.10	-0.19	+0.97	93.43	-4.56	88.87
$\text{HCl}^- + \text{CH}_2\text{I}$	103.87	-0.33	-0.03	+0.15	103.66	-8.72	94.95
$\text{I}^- + \text{HCl} + \text{CH}_2^h$	91.36	-0.30	+0.11	+1.28	92.45	-8.24	84.20

^aThe detailed FPA tables and the structures of the stationary points are given in the SI. All the single-point energy computations are performed at the all-electron CCSD(T)/aug-cc-pwCVTZ geometries. For iodine, an effective core potential and the corresponding PP basis set are used.

^bComplete basis set limits of the CCSD(T) energies obtained from the aug-cc-pVQZ and aug-cc-pVSZ results using two-parameter extrapolation formulas given in eqs 1 and 2. ^cPost-CCSD(T) correlation energy increments obtained as $\delta[\text{CCSDT}] = \text{CCSDT} - \text{CCSD(T)}$ and $\delta[\text{CCSDT(Q)}] = \text{CCSDT(Q)} - \text{CCSDT}$ with the aug-cc-pVDZ basis. ^dCore correlation energy corrections obtained from all-electron and frozen-core computations at the CCSD(T)/aug-cc-pwCVQZ level of theory. ^eBenchmark classical FPA energies obtained as $\text{CCSD(T)/CBS} + \delta[\text{CCSDT}] + \delta[\text{CCSDT(Q)}] + \Delta\text{core}$. ^fZero-point energy corrections obtained at the CCSD(T)-F12b/aug-cc-pVTZ level of theory. ^gBenchmark adiabatic FPA energies obtained as $\text{CCSD(T)/CBS} + \delta[\text{CCSDT}] + \delta[\text{CCSDT(Q)}] + \Delta\text{core} + \Delta\text{ZPE}$. ^hThese data correspond to the singlet (excited) electronic state of CH_2 , because a singlet PES adiabatically correlates to singlet CH_2 .

Hartree–Fock (HF),³⁶ second-order Møller–Plesset perturbation theory (MP2),³⁷ CCSD,³⁸ CCSD(T),²⁸ coupled-cluster singles, doubles, and triples [CCSDT],³⁹ and coupled-cluster singles, doubles, triples, and perturbative quadruples [CCSDT-(Q)]⁴⁰ methods. Up to CCSD(T) the aug-cc-pVnZ [$n = 2(\text{D}), 3(\text{T}), 4(\text{Q}), 5$] basis sets are used, whereas the aug-cc-pVDZ basis is employed for the extremely time-consuming CCSDT and CCSDT(Q) computations.

The complete basis set (CBS) limits of the HF energies are obtained by^{41–43}

$$E_n^{\text{HF}} = E_{\text{CBS}}^{\text{HF}} + a(n+1)e^{-9\sqrt{n}} \quad (1)$$

where E_n^{HF} are the HF/aug-cc-pVnZ energies and $E_{\text{CBS}}^{\text{HF}}$ is the HF CBS limit. The correlation energy increments, defined as $\delta[\text{MP2}] = E[\text{MP2}] - E[\text{HF}]$, $\delta[\text{CCSD}] = E[\text{CCSD}] - E[\text{MP2}]$, and $\delta[\text{CCSD(T)}] = E[\text{CCSD(T)}] - E[\text{CCSD}]$, are extrapolated to the corresponding CBS limits, $E_{\text{CBS}}^{\text{corr}}$, using⁴⁴

$$E_n^{\text{corr}} = E_{\text{CBS}}^{\text{corr}} + bn^{-3} \quad (2)$$

where E_n^{corr} is $E_n^{\text{MP2}} - E_n^{\text{HF}}$, $E_n^{\text{CCSD}} - E_n^{\text{MP2}}$, and $E_n^{\text{CCSD(T)}} - E_n^{\text{CCSD}}$, respectively. Both eqs 1 and 2 have two parameters ($E_{\text{CBS}}^{\text{HF}}$ and a) and ($E_{\text{CBS}}^{\text{corr}}$ and b), which are determined using the aug-cc-pVnZ [$n = 4(\text{Q})$ and 5] data. Note that when using eq 2 it does not matter if we extrapolate the relative correlation energies or compute the relative energies from the extrapolated absolute

correlation energy increments; thus, symbol δ can refer to absolute and relative energy increments as well. The CCSD(T)/CBS energy is obtained as $\text{HF/CBS} + \delta[\text{MP2/CBS}] + \delta[\text{CCSD/CBS}] + \delta[\text{CCSD(T)/CBS}]$.

The benchmark classical relative energies of the stationary points are obtained at the AE-CCSD(T)/aug-cc-pwCVTZ geometries as

$$\Delta E(\text{CCSD(T)/CBS}) + \delta[\text{CCSDT}] + \delta[\text{CCSDT(Q)}] + \Delta\text{core} \quad (3)$$

where the post-CCSD(T) correlation effects are computed with the aug-cc-pVDZ basis as $\delta[\text{CCSDT}] = \Delta E[\text{CCSDT}] - \Delta E[\text{CCSD(T)}]$ and $\delta[\text{CCSDT(Q)}] = \Delta E[\text{CCSDT(Q)}] - \Delta E[\text{CCSDT}]$, and Δcore denotes the core electron correlation correction obtained as the difference between all-electron and frozen-core CCSD(T)/aug-cc-pwCVQZ energies.

Finally, the benchmark adiabatic relative energies are defined as

$$\Delta E(\text{CCSD(T)/CBS}) + \delta[\text{CCSDT}] + \delta[\text{CCSDT(Q)}] + \Delta\text{core} + \Delta\text{ZPE} \quad (4)$$

where the zero-point energy corrections (ΔZPE) are computed at the CCSD(T)-F12b/aug-cc-pVTZ level of theory.

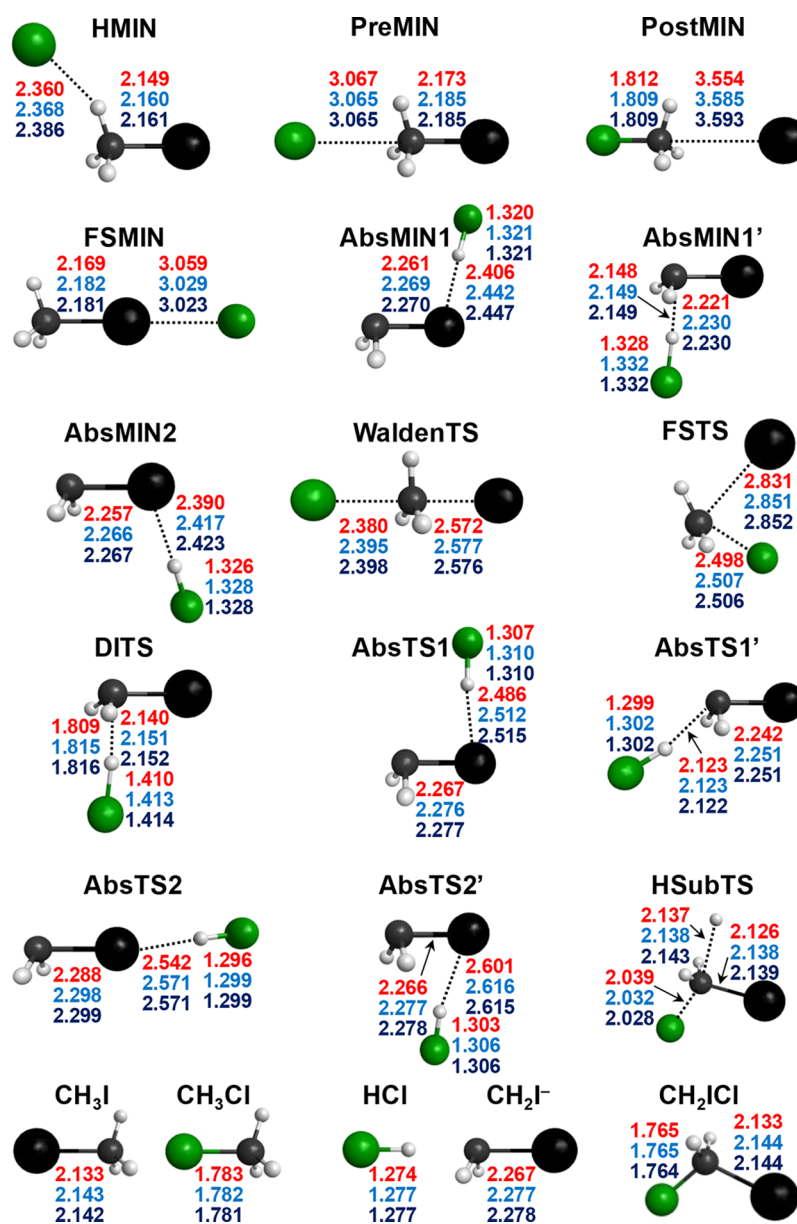


Figure 2. Structures of the minima, transition states, and various products corresponding to the $\text{Cl}^- + \text{CH}_3\text{I}$ reaction showing the most important distances (Å) obtained at the AE-CCSD(T)/aug-cc-pwCVTZ (red), CCSD(T)-F12b/aug-cc-pVTZ (blue), and CCSD(T)-F12b/aug-cc-pVQZ (dark blue) levels of theory, from up to down, respectively.

All the above electronic structure computations up to CCSD(T) are performed with the Molpro ab initio package.⁴⁵ The CCSDT and CCSDT(Q) energies are obtained by the MRCC program⁴⁶ interfaced to Molpro.

III. RESULTS AND DISCUSSION

The schematic potential energy surface of the $\text{Cl}^- + \text{CH}_3\text{I}$ reaction showing the different reaction pathways and the corresponding complexes and transition states are given in Figure 1. The back-side attack $\text{S}_{\text{N}}2$ pathway goes through a prereaction ion-dipole complex (PreMIN, $-11.56/-11.42$), followed by an inversion via the WaldenTS ($-5.48/-5.54$), resulting in a postreaction complex (PostMIN, $-23.66/-22.72$), which dissociates to the $\text{I}^- + \text{CH}_3\text{Cl}$ products ($-14.88/-14.07$). The above benchmark classical/adiabatic energies, in kcal/mol, relative to the reactants show that the $\text{Cl}^- + \text{CH}_3\text{I}$ $\text{S}_{\text{N}}2$ reaction is exothermic with a slightly submerged

barrier. Besides the well-known PreMIN complex, we have also found a hydrogen-bonded complex (HMIN, $-10.81/-10.57$). HMIN-type complexes were previously reported for F^- and OH^- nucleophiles,^{11,12,6,8,9} where HMIN is usually a deeper minimum than PreMIN. In the present case, HMIN has slightly higher energy than PreMIN in accord with the expectation that chlorine does not favor hydrogen bonds. Based on our previous studies,⁶⁻⁹ HMIN and PreMIN must be connected via a first-order saddle point (HTS), but we could not get a converged structure for this transition state using the MP2, CCSD(T), CCSD(T)-F12a, and CCSD(T)-F12b methods with the aug-cc-pVDZ basis and the CCSD(T) method with aug-cc-pVTZ. Besides the back-side complexes, we also found a front-side complex (FSMIN, $-9.26/-9.32$), where Cl^- connects to the I atom of the reactant. In the case of $\text{F}^- + \text{CH}_3\text{I}$, FSMIN is even deeper than PreMIN, whereas for $\text{F}^- + \text{CH}_3\text{Cl}$, FSMIN is shallow, only ~ 3 kcal/mol deep minimum.^{13,14} In the present

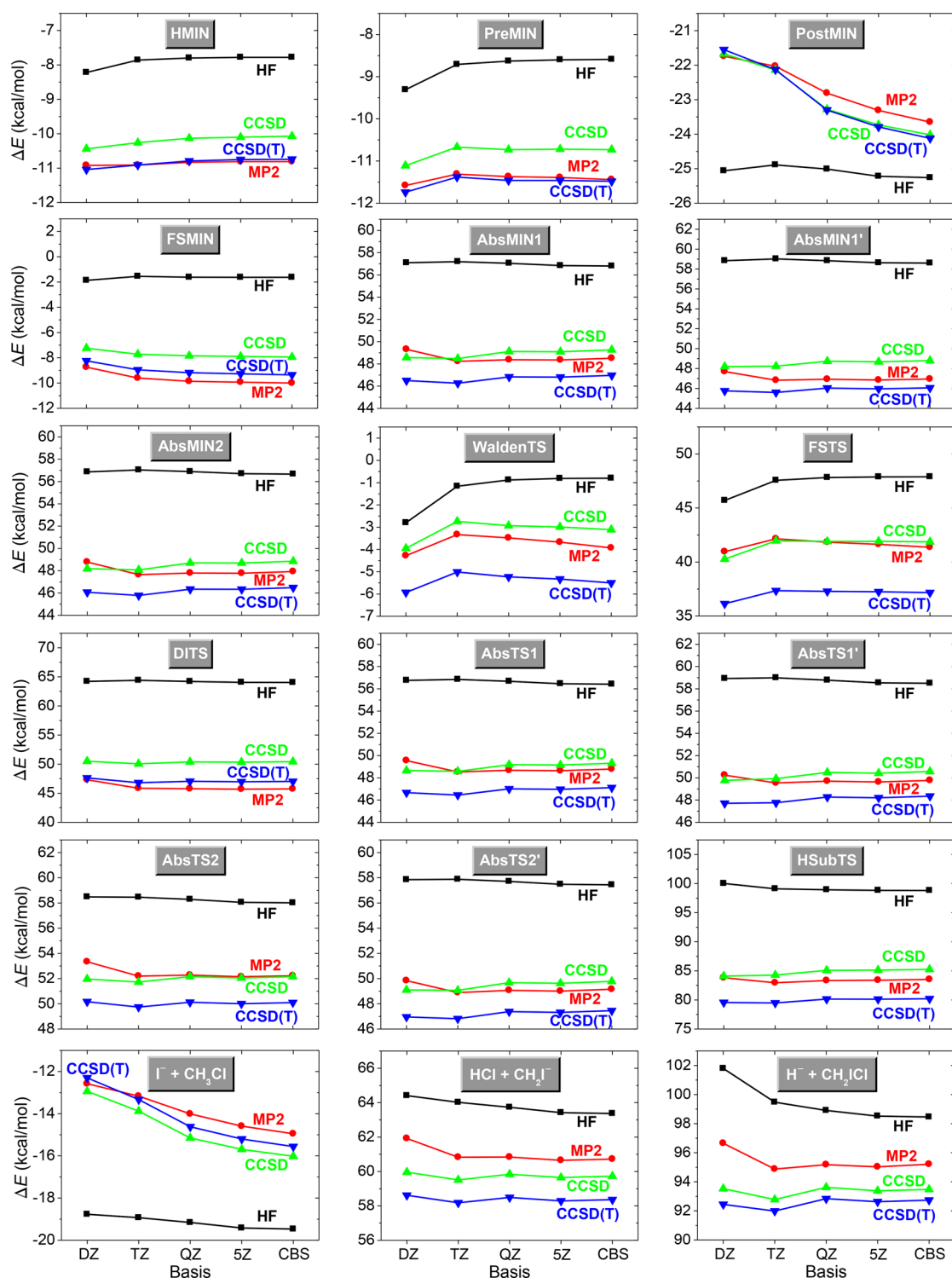


Figure 3. Method and basis set (aug-cc-pVnZ, $n = D, T, Q, 5$, and CBS, complete basis set) dependence of the classical energies, relative to the reactants, of the stationary points (shown in Figures 1 and 2) of the $\text{Cl}^- + \text{CH}_3\text{I}$ reaction.

$\text{Cl}^- + \text{CH}_3\text{I}$ case, the depth of FSMIN is significant, although PreMIN is slightly deeper. The front-side complexes of the $\text{OH}^- + \text{CH}_3\text{I}$ ⁴⁷ and $\text{F}^- + \text{CH}_3\text{Y}$ [$\text{Y} = \text{Cl}, \text{I}$]¹⁴ reactions were recently studied by detailed dynamics simulations. The latter work revealed significant front-side complex formation in the $\text{F}^- + \text{CH}_3\text{I}$ $\text{S}_{\text{N}}2$ reaction.¹⁴

The $\text{Cl}^- + \text{CH}_3\text{I}$ $\text{S}_{\text{N}}2$ reaction can also proceed via a front-side attack transition state (FSTS, 36.73/35.89), resulting in products without inversion. Another possible retention pathway

is the double inversion via DITS (46.97/42.55). As seen, both retention mechanisms have high barriers, and unlike in the case of F^- nucleophile, for $\text{Cl}^- + \text{CH}_3\text{I}$ the FSTS is below the DITS. This may be explained by the fact that F^- has larger proton affinity than Cl^- ; thus, the proton abstraction is energetically less favored in the title reaction. Since the first step of double inversion is a proton-abstraction-induced inversion, the DITS is expected to have higher relative energy in the case of Cl^- nucleophile. The first inversion of the double inversion process

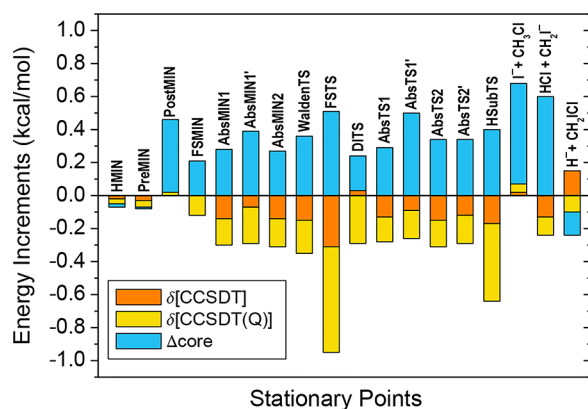


Figure 4. Post-CCSD(T) and core correlation contributions to the relative energies of the stationary points (shown in Figures 1 and 2) of the $\text{Cl}^- + \text{CH}_3\text{I}$ reaction. $\delta[\text{CCSDT}] = \text{CCSDT} - \text{CCSD(T)}$ and $\delta[\text{CCSDT(Q)}] = \text{CCSDT(Q)} - \text{CCSDT}$ are computed with the aug-cc-pVDZ basis, and Δ_{core} is obtained from all-electron and frozen-core computations at the CCSD(T)/aug-cc-pwCVQZ level of theory.

is followed by a second inversion via the usual WaldentTS resulting in overall retention. It is also possible that the first inversion is not followed by a reactive substitution event, but the reaction results in an inverted reactant. This mechanism is called induced inversion as indicated in Figure 1. We must note that double inversion may proceed via a nonintrinsic reaction coordinate (non-IRC) pathway as suggested previously in the case of the $\text{F}^- + \text{CH}_3\text{I}$ reaction.²⁴ Thus, the investigation of the role of the DITS in the double-inversion mechanism is an interesting future research direction.

Besides the $\text{S}_{\text{N}}2$ channel, the $\text{Cl}^- + \text{CH}_3\text{I}$ reaction has several endothermic product channels such as $\text{HCl} + \text{CH}_2\text{I}^-$ (58.72/53.54), $\text{H}^- + \text{CH}_2\text{ICI}$ (92.65/87.47), $\text{I}^- \cdots \text{HCl} + \text{CH}_2(\bar{a}^1\text{A}_1)$ (77.40/69.75), $\text{ICI}^- + \text{CH}_3$ (38.00/33.99), $\text{ICI} + \text{CH}_3^-$ (93.43/88.87), $\text{HCl}^- + \text{CH}_2\text{I}$ (103.66/94.95), and $\text{I}^- + \text{HCl} + \text{CH}_2(\bar{a}^1\text{A}_1)$ (92.45/84.20) as given in Table 1. For the proton transfer channel leading to $\text{HCl} + \text{CH}_2\text{I}^-$, we have located several minima and transition states in the postreaction well below the product asymptote as shown in Figure 1. These stationary points have similar structures as the corresponding minima and TSs of the $\text{F}^- + \text{CH}_3\text{I}$ reaction,^{24,9} but the present energies are shifted toward the more endothermic region of 40–50 kcal/mol. For the highly endothermic hydride-substitution channel, we have found a first-order saddle point (HSubTS, 79.97/74.95), whose energy is below the energy level of the $\text{H}^- + \text{CH}_2\text{ICI}$ products as also shown in Figure 1. For the additional product channels we have just determined the reaction enthalpies as given in Table 1. These benchmark data could be especially useful in future PES developments for the title reaction. Among these channels the halide abstraction leading to two doublet products, $\text{ICI}^- + \text{CH}_3$, may be the most important because this channel has the lowest endothermicity, even lower than the proton-abstraction channel. Note that the two singlet products, $\text{ICI} + \text{CH}_3^-$, have about 50 kcal/mol larger energy than $\text{ICI}^- + \text{CH}_3$. For $\text{HCl} + \text{CH}_2\text{I}^-$ we have also checked that exchange of the negative charge, i.e., $\text{HCl}^- + \text{CH}_2\text{I}$, increases the energy by more than 40 kcal/mol. About the $\text{I}^- \cdots \text{HCl} + \text{CH}_2$ product channel, which eventually leads to $\text{I}^- + \text{HCl} + \text{CH}_2$, we must note that only singlet CH_2 can be formed on a singlet PES of the $\text{Cl}^- + \text{CH}_3\text{I}$ system because the ground electronic states of $\text{I}^- \cdots \text{HCl}$, I^- , and HCl are singlet. Therefore, in Table 1, the relative energies correspond to

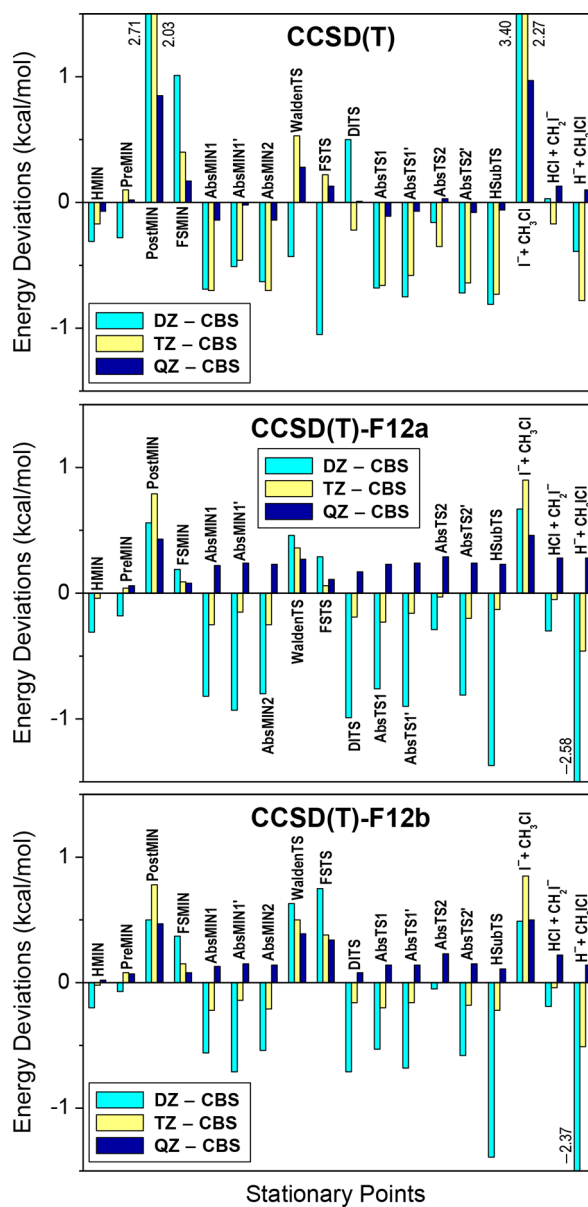


Figure 5. Deviations of the relative energies of the stationary points (shown in Figures 1 and 2) obtained with different frozen-core CCSD(T) methods with the aug-cc-pVDZ (DZ), aug-cc-pVTZ (TZ), and aug-cc-pVQZ (QZ) basis sets with respect to the CCSD(T)/complete-basis-set (CBS) results.

singlet CH_2 , even if the ground electronic state of CH_2 is triplet. Of course, in a nonadiabatic process triplet CH_2 can be formed, whose energy is lower by ~ 9 kcal/mol than the energy of the singlet state.⁴⁸

The structures of most of the above-mentioned stationary points are given in Figure 2, showing the most important structural parameters obtained with the AE-CCSD(T)/aug-cc-pwCVTZ and CCSD(T)-F12b/aug-cc-pVnZ [$n = \text{T}$ and Q] levels of theory. Furthermore, all the internal coordinates at 11 different theoretical levels for all the stationary points considered in this study are given in Tables S1–S24 in the Supporting Information (SI). Here, we just highlight a few interesting observations. Although the DITS seems similar to the proton-abstraction stationary points, unique differences exist such as (1) the HCl distance of the DITS is stretched by 0.137 Å relative to the bond length of the HCl molecule,

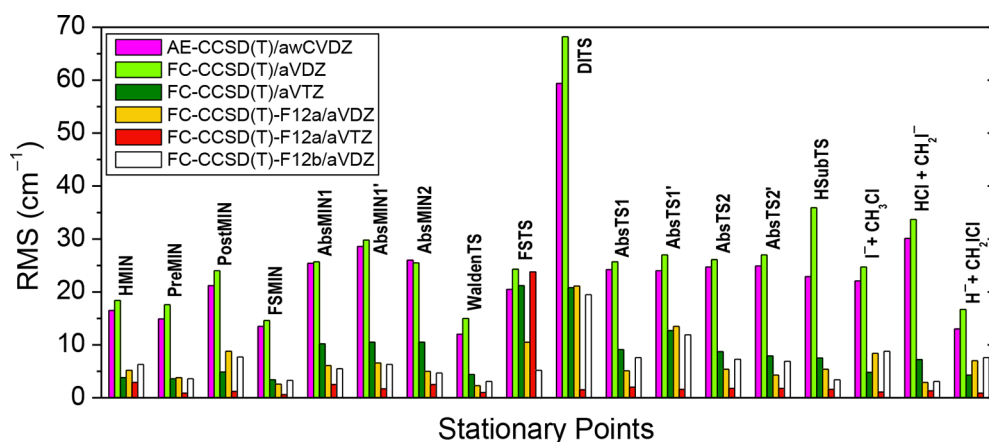


Figure 6. Root-mean-square deviations of the harmonic vibrational frequencies of the stationary points (shown in Figures 1 and 2) obtained with different all-electron (AE) and frozen-core (FC) levels of theory with respect to the CCSD(T)-F12b/aug-cc-pVTZ results.

whereas the corresponding stretchings are between 0.022 and 0.055 Å for all the abstraction structures, and (2) the H...C distance is about 1.8 Å at the DITS, whereas always larger than 2.1 Å for the other abstraction-like structures. Regarding the accuracy of the structures, Figure 2 shows that the CCSD(T)-F12b distances with aug-cc-pVTZ and aug-cc-pVQZ bases usually agree within 0.001 Å, except for some of the long interfragment distances. The largest deviation of 0.008 Å is seen at the PostMIN complex. The AE-CCSD(T)/aug-cc-pwCVDZ distances usually differ from the frozen-core CCSD(T)-F12b results by about 0.01 Å. This difference comes from two major sources, namely, the F12b results are better converged with respect to the basis set, whereas the present F12b computations neglect the correlation of the core electrons. In some cases, where the former effect is more important than the latter, the CCSD(T)-F12b results are more accurate, and in other cases, the AE-CCSD(T) distances are more definitive. An example for the latter case is the I...C distance of FSTS, where the AE value is converged within about 0.002 Å and below the frozen-core value by about 0.02 Å. (Note that the uncertainty of the structural parameters can be predicted based on the detailed data given in Tables S1–S24.)

The benchmark classical and adiabatic relative energies of the minima, transition states, and various product channels are summarized in Table 1, and the corresponding detailed focal-point analysis tables are given in the SI. The graphical representations of most focal-point tables, i.e., the method and basis set dependence of the relative energies and the post-CCSD(T) and core correlation effects, are shown in Figures 3 and 4, respectively. As seen in Figure 3 in most cases the method dependence is more important than the basis set dependence. The HF method usually seriously overestimates the relative energies, except for the product-type structures, where it seriously underestimates. As Figure 3 shows, the error of the HF method can be as large as 10 kcal/mol; thus, the HF results are very far from chemical accuracy, usually considered 1 kcal/mol, for the title reaction and similar systems. MP2 greatly improves the accuracy of the relative energies, and in many cases, for example, see HMIN and PreMIN in Figure 3, the MP2 and CCSD(T) data agree within 1 kcal/mol. In fact, in many cases CCSD does not improve the MP2 results; see, for example, HMIN, PreMIN, WaldenTS, etc. Of course, it is not a general rule since, for example, for the HCl + CH₂I⁻ and H⁻ + CH₂Cl product channels, a monotonic HF → MP2 → CCSD

→ CCSD(T) convergence is seen. The basis set incompleteness errors are usually small. In some cases the DZ and TZ results deviate by 1 kcal/mol, as seen, for example, for the WaldenTS, but the TZ and CBS energies usually agree within 0.5 kcal/mol. The most serious basis set dependence is found for the I⁻ + CH₃Cl product channel, where the CCSD(T)/aug-cc-pVDZ relative energy is higher than the CBS limit by 3.26 kcal/mol. A similar large DZ vs CBS basis set effect of 2.57 kcal/mol is found for the product-type PostMIN complex. Comparing the 5Z and CBS CCSD(T) energies, the differences are only 0.36 and 0.33 kcal/mol for I⁻ + CH₃Cl and PostMIN, respectively; thus, the CBS data are converged within about 0.2 kcal/mol even for these problematic cases. (Note that the qualitatively different method and basis dependence found for the PreMIN and PostMIN complexes are due to the fact the energies of both minima are relative to Cl⁻ + CH₃I. The trends would be similar in both cases if the energy of the product-type PostMIN were relative to I⁻ + CH₃Cl.) For most of the stationary points, the CCSD(T)/CBS results are basis set converged within 0.1 kcal/mol.

As Table 1 and Figure 4 show, the $\delta[\text{CCSDT}]$ and $\delta[\text{CCSDT}(Q)]$ correlation energy increments usually have the same negative sign, resulting in post-CCSD(T) correlation effects in the range from 0.0 to -0.4 kcal/mol. The effects are negligible for the complexes such as HMIN, PreMIN, and PostMIN, whereas the increments are more significant for the WaldenTS (-0.35 kcal/mol), DITS (-0.26 kcal/mol), etc. (see Figure 4). The largest post-CCSD(T) effect of -0.95 kcal/mol is found for the FSTS, which certainly cannot be neglected if high accuracy is desired. The correlation effects beyond CCSDT(Q) are expected to be an order of magnitude smaller than $\delta[\text{CCSDT}(Q)]$; thus, usually well below 0.1 kcal/mol. The core correlation corrections have similar magnitudes, but opposite signs as the post-CCSD(T) effects (see Figure 4). Therefore, in many cases the two effects cancel each other. This means that the frozen-core CCSD(T)/CBS energies are of high accuracy without post-CCSD(T) and core corrections. This finding alerts everyone that it is not worth performing all-electron CCSD(T) computations without considering post-CCSD(T) correlation effects, and there is no need for computing electron correlation energies beyond CCSD(T) without taking account of the correlation of the core electrons. (Note that post-CCSD(T) correlation energies can/should be computed using the frozen-core approach, and it is usually

sufficient to determine the core correlation corrections at the CCSD(T) level.) The above finding about the fortuitous energy cancelation is not unique for the title reaction, but rather general, for example, we found very similar behavior for the $F + CH_4$ and $O + CH_4$ systems.⁴⁹ Of course, we can find examples where one cannot avoid performing the demanding CCSDT(Q) and all-electron computations if aiming for high accuracy because, for instance, in the case of the $I^- + CH_3Cl$ product channel, the post-CCSD(T) and core corrections are both positive and add up to 0.68 kcal/mol as seen in Table 1.

As discussed above, the CBS extrapolation, the correlation treatment up to CCSDT(Q), and the core correlation effects are all well converged in the present study; thus, we expect that most of the classical relative energies present in Table 1 have uncertainties less than 0.1–0.2 kcal/mol. In order to determine the adiabatic energies, the ZPE corrections have to be added to the classical values. As Table 1 shows, the ZPE effects are not negligible and in some cases quite substantial. For the prereaction complexes, HMIN, PreMIN, and FSMIN, the ZPE effects are relatively small, around 0.1–0.2 kcal/mol. For the WaldenTS, the ZPE correction is also small, -0.06 kcal/mol, whereas for the FSTS it is somewhat larger (-0.84 kcal/mol). For the DITS, a much more significant ZPE effect is found decreasing the double-inversion barrier height by 4.42 kcal/mol. For the proton-abstraction stationary points and products similar, large ZPE corrections are obtained. For the S_N2 products, the ZPE correction is positive (0.81 kcal/mol) because the ZPE of CH_3Cl is larger than that of CH_3I . For the endothermic product channels the ZPE corrections decrease the reaction enthalpies, in some cases quite substantially by 5–9 kcal/mol. Note that the uncertainties of the present adiabatic relative energies are larger than those of the classical values due to the neglected anharmonic effects. Performing anharmonic vibrational analysis for the present six-atomic complexes and transition states would be extremely challenging, and this is obviously out of the scope of the present study. Nevertheless, in the case of the $I^- + CH_3Cl$ product channel we can check the accuracy of our prediction using the enthalpy of formation data taken from the Active Thermochemical Tables (ATcT).⁵⁰ Utilizing the 0 K enthalpies of formation of -44.93 ± 0.00 (I^-), -17.75 ± 0.06 (CH_3Cl), -54.72 ± 0.00 (Cl^-), and 5.85 ± 0.04 (CH_3I) kcal/mol, based on version 1.122 of the Thermochemical Network (2016),⁵¹ an enthalpy of -13.81 ± 0.07 kcal/mol is obtained for the $Cl^- + CH_3I \rightarrow I^- + CH_3Cl$ reaction. This is in good agreement with the present adiabatic energy of -14.07 kcal/mol. Furthermore, we note that in the version 1.118 (2015),⁵² the enthalpy of formation of CH_3Cl is -17.86 ± 0.05 kcal/mol, which results in a reaction enthalpy of -13.92 ± 0.06 kcal/mol, in even better agreement with the present value.

Focal-point analysis, as was done in the present study, is not commonly applied to S_N2 reactions. One rather chooses an electronic structure method and basis and then optimizes the geometries and determines the relative energies. The present benchmark data allows testing the accuracy of this approach in the case of several ab initio levels of theory. Figure 5 shows the performance of the CCSD(T), CCSD(T)-F12a, and CCSD(T)-F12b methods with the aug-cc-pVnZ [$n = 2(D), 3(T), 4(Q)$] bases with respect to the CCSD(T)/CBS relative energies. For the title reaction the standard CCSD(T) with aug-cc-pVDZ performs surprisingly well since most of the relative energies are chemically accurate (the deviations from the CBS data are less than 1 kcal/mol). It is somewhat unusual because the standard correlation methods with aug-cc-pVDZ

basis can give errors of 2–3 kcal/mol.⁴⁹ Of course, we must note that we found two cases, PostMIN and $I^- + CH_3Cl$, where the errors are 2.71 and 3.40 kcal/mol, respectively, and the aug-cc-pVQZ basis is needed to reduce the error below 1 kcal/mol. For these two stationary points, the F12 methods are extremely advantageous because both F12a and F12b give ~ 0.5 kcal/mol accuracy with the aug-cc-pVDZ basis. It is generally true that the F12a and F12b methods perform similarly, but unexpectedly, the F12 methods do not show significant improvement of the corresponding standard CCSD(T) results in the case of most of the stationary points investigated in the present study.

Figure 6 shows the accuracy of the harmonic vibrational frequencies obtained with different levels of theory with respect to the CCSD(T)-F12b/aug-cc-pVTZ results. Here, the standard CCSD(T) with aug-cc-pVDZ clearly performs the worst resulting in 20–30 cm^{-1} root-mean-square errors. The F12 methods significantly improve the CCSD(T)/aug-cc-pVDZ frequencies reducing the errors usually below 10 cm^{-1} . The CCSD(T)-F12a/b methods with aug-cc-pVDZ actually give similar frequencies as CCSD(T)/aug-cc-pVTZ; moreover, the former methods sometimes outperform the more time-consuming latter. The comparison of all-electron and frozen-core results shows that the core electron correlation does not have significant effects on the frequencies. Thus, the message of Figure 6 is that the frozen-core CCSD(T)-F12a or CCSD(T)-F12b method with the aug-cc-pVDZ basis is recommended for frequency computations for 6–10-atomic S_N2 reactions.

IV. SUMMARY AND CONCLUSIONS

Motivated by the recent experimental and theoretical findings on the dynamics of S_N2 reactions, we have reported a detailed ab initio investigation of the stationary points of the PES of the $Cl^- + CH_3I$ reaction. The present study provides new qualitative as well as quantitative insights into the chemistry of the title reaction. On the qualitative side, new stationary points are revealed for the $Cl^- + CH_3I$ reaction, for example, many $ClH \cdots CH_2I^-$ -type complexes and transition states. The S_N2 reaction can proceed via back-side attack inversion as well as front-side attack and double-inversion retention pathways. Among the retention mechanisms, the front-side attack has a lower barrier, unlike in the case of F^- nucleophile. On the quantitative side, we have provided benchmark structures, frequencies, and relative energies for the minima, transition states, and various product channels. The best technically feasible relative energies are obtained by a two-dimensional extrapolation scheme, called focal-point analysis, considering the systematic improvement of (1) the ab initio treatment of electron correlation via $HF \rightarrow MP2 \rightarrow CCSD \rightarrow CCSD(T) \rightarrow CCSDT \rightarrow CCSDT(Q)$ and (2) the size of the basis set as $n = 2(D) \rightarrow 3(T) \rightarrow 4(Q) \rightarrow 5$ in aug-cc-pVnZ. We found that electron correlation plays an important role in the accurate determination of the energetics of the title reaction, whereas the results often show moderate basis set dependence. The post-CCSD(T) correlation and core electron correlation effects often have the same magnitude of about 0.4 kcal/mol, but due to their opposite signs, these auxiliary corrections can cancel each other. The CCSD(T)-F12 methods with the aug-cc-pVDZ basis are found very efficient for geometry and frequency computations. For energy computations, the advantage of the F12 methods is not significant, due to the fact that in most case the relative energies do not have serious basis set dependence. Of course, this is not a general statement, and even in the

present work, we found some stationary points where the basis set dependence was strong and the F12 methods greatly improved the convergence of the relative energies.

The benchmark data reported for stationary points will hopefully motivate and help future experimental and theoretical studies of the title reaction. For example, the ab initio characterization of the minima, transition states, and product asymptotes is the first step toward an analytical PES development for a chemical reaction. We plan to develop such a PES for the title reaction in the near future, which will allow efficient dynamics simulations. Furthermore, the strategies used in the present study to obtain accurate ab initio data could be utilized by others studying similar systems.

■ ASSOCIATED CONTENT

Supporting Information

The Supporting Information is available free of charge on the ACS Publications website at DOI: 10.1021/acs.jpca.7b05503.

Energies, structural parameters, harmonic zero-point energies, and vibrational fundamentals of all the stationary points computed at different levels of theory as well as benchmark classical relative energies obtained with the focal-point analysis approach (PDF)

■ AUTHOR INFORMATION

Corresponding Author

*E-mail: gczako@chem.u-szeged.hu.

ORCID

István Szabó: 0000-0002-3700-3614

Gábor Czakó: 0000-0001-5136-4777

Present Address

†Department of Chemistry, King's College London, London SE1 1DB, United Kingdom.

Notes

The authors declare no competing financial interest.

■ ACKNOWLEDGMENTS

G.C. thanks the Scientific Research Fund of Hungary (PD-111900) and the János Bolyai Research Scholarship of the Hungarian Academy of Sciences for financial support. We acknowledge the National Information Infrastructure Development Institute for awarding us access to resources based in Hungary at Debrecen and Szeged.

■ REFERENCES

- (1) Glukhovtsev, M. N.; Pross, A.; Radom, L. Gas-Phase Identity S_N2 Reactions of Halide Anions with Methyl Halides: A High-Level Computational Study. *J. Am. Chem. Soc.* **1995**, *117*, 2024–2032.
- (2) Glukhovtsev, M. N.; Pross, A.; Radom, L. Gas-Phase Non-Identity S_N2 Reactions of Halide Anions with Methyl Halides: A High-Level Computational Study. *J. Am. Chem. Soc.* **1996**, *118*, 6273–6284.
- (3) Parthiban, S.; de Oliveira, G.; Martin, J. M. L. Benchmark ab Initio Energy Profiles for the Gas-Phase S_N2 Reactions $Y^- + CH_3X \rightarrow CH_3Y + X^-$ ($X, Y = F, Cl, Br$). Validation of Hybrid DFT Methods. *J. Phys. Chem. A* **2001**, *105*, 895–904.
- (4) Gonzales, J. M.; Cox, R. S.; Brown, S. T.; Allen, W. D.; Schaefer, H. F. Assessment of Density Functional Theory for Model S_N2 Reactions: $CH_3X + F^-$ ($X = F, Cl, CN, OH, SH, NH_2, PH_2$). *J. Phys. Chem. A* **2001**, *105*, 11327–11346.
- (5) Gonzales, J. M.; Pak, C.; Cox, R. S.; Allen, W. D.; Schaefer, H. F., III; Császár, A. G.; Tarczay, G. Definitive ab Initio Studies of Model S_N2 Reactions $CH_3X + F^-$ ($X = F, Cl, CN, OH, SH, NH_2, PH_2$). *Chem. - Eur. J.* **2003**, *9*, 2173–2192.

(6) Szabó, I.; Császár, A. G.; Czakó, G. Dynamics of the $F^- + CH_3Cl \rightarrow Cl^- + CH_3F$ S_N2 Reaction on a Chemically Accurate Potential Energy Surface. *Chem. Sci.* **2013**, *4*, 4362–4370.

(7) Szabó, I.; Czakó, G. Revealing a Double-Inversion Mechanism for the $F^- + CH_3Cl$ S_N2 Reaction. *Nat. Commun.* **2015**, *6*, 5972.

(8) Szabó, I.; Telekes, H.; Czakó, G. Accurate ab Initio Potential Energy Surface, Thermochemistry, and Dynamics of the $F^- + CH_3F$ S_N2 and Proton-Abstraction Reactions. *J. Chem. Phys.* **2015**, *142*, 244301.

(9) Olasz, B.; Szabó, I.; Czakó, G. High-Level ab Initio Potential Energy Surface and Dynamics of the $F^- + CH_3I$ S_N2 and Proton-Transfer Reactions. *Chem. Sci.* **2017**, *8*, 3164–3170.

(10) Xie, J.; Hase, W. L. Rethinking the S_N2 Reaction. *Science* **2016**, *352*, 32–33.

(11) Zhang, J.; Mikosch, J.; Trippel, S.; Otto, R.; Weidemüller, M.; Wester, R.; Hase, W. L. $F^- + CH_3I \rightarrow FCH_3 + I^-$ Reaction Dynamics. Nontraditional Atomistic Mechanisms and Formation of a Hydrogen-Bonded Complex. *J. Phys. Chem. Lett.* **2010**, *1*, 2747–2752.

(12) Xie, J.; Zhang, J.; Hase, W. L. Is There Hydrogen Bonding for Gas Phase S_N2 Pre-Reaction Complexes? *Int. J. Mass Spectrom.* **2015**, *378*, 14–19.

(13) Stei, M.; Carrascosa, E.; Kainz, M. A.; Kelkar, A. H.; Meyer, J.; Szabó, I.; Czakó, G.; Wester, R. Influence of the Leaving Group on the Dynamics of a Gas-Phase S_N2 Reaction. *Nat. Chem.* **2016**, *8*, 151–156.

(14) Szabó, I.; Olasz, B.; Czakó, G. Deciphering Front-Side Complex Formation in S_N2 Reactions via Dynamics Mapping. *J. Phys. Chem. Lett.* **2017**, *8*, 2917–2923.

(15) Glukhovtsev, M. N.; Pross, A.; Schlegel, H. B.; Bach, R. D.; Radom, L. Gas-Phase Identity S_N2 Reactions of Halide Anions and Methyl Halides with Retention of Configuration. *J. Am. Chem. Soc.* **1996**, *118*, 11258–11264.

(16) Angel, L. A.; Ervin, K. M. Dynamics of the Gas-Phase Reactions of Fluoride Ions with Chloromethane. *J. Phys. Chem. A* **2001**, *105*, 4042–4051.

(17) Bento, A. P.; Bickelhaupt, F. M. Nucleophilicity and Leaving-Group Ability in Frontside and Backside S_N2 Reactions. *J. Org. Chem.* **2008**, *73*, 7290–7299.

(18) Ingold, C. K. *Structure and Mechanisms in Organic Chemistry*; Cornell Univ. Press: Ithaca, NY, 1953.

(19) Szabó, I.; Czakó, G. Double-Inversion Mechanisms of the $X^- + CH_3Y$ [$X, Y = F, Cl, Br, I$] S_N2 Reactions. *J. Phys. Chem. A* **2015**, *119*, 3134–3140.

(20) Szabó, I.; Czakó, G. Mode-Specific Multi-Channel Dynamics of the $F^- + CHD_2Cl$ Reaction on a Global ab Initio Potential Energy Surface. *J. Chem. Phys.* **2016**, *145*, 134303.

(21) Liu, P.; Wang, D. Y.; Xu, Y. A New, Double-Inversion Mechanism of the $F^- + CH_3Cl$ S_N2 Reaction in Aqueous Solution. *Phys. Chem. Chem. Phys.* **2016**, *18*, 31895–31903.

(22) Liu, P.; Zhang, J.; Wang, D. Y. Multi-Level Quantum Mechanics Theories and Molecular Mechanics Study of the Double-Inversion Mechanism of the $F^- + CH_3I$ Reaction in Aqueous Solution. *Phys. Chem. Chem. Phys.* **2017**, *19*, 14358–14365.

(23) Tajti, V.; Czakó, G. Benchmark ab Initio Characterization of the Complex Potential Energy Surface of the $F^- + CH_3CH_2Cl$ Reaction. *J. Phys. Chem. A* **2017**, *121*, 2847–2854.

(24) Zhang, J.; Xie, J.; Hase, W. L. Dynamics of the $F^- + CH_3I \rightarrow HF + CH_2I^-$ Proton Transfer Reaction. *J. Phys. Chem. A* **2015**, *119*, 12517–12525.

(25) Mikosch, J.; Trippel, S.; Eichhorn, C.; Otto, R.; Lourderaj, U.; Zhang, J.-X.; Hase, W. L.; Weidemüller, M.; Wester, R. Imaging Nucleophilic Substitution Dynamics. *Science* **2008**, *319*, 183–186.

(26) Zhang, J.; Lourderaj, U.; Sun, R.; Mikosch, J.; Wester, R.; Hase, W. L. Simulation Studies of the $Cl^- + CH_3I$ S_N2 Nucleophilic Substitution Reaction: Comparison with Ion Imaging Experiments. *J. Chem. Phys.* **2013**, *138*, 114309.

(27) Zhang, J.; Lourderaj, U.; Addepalli, S. V.; de Jong, W. A.; Hase, W. L. Quantum Chemical Calculations of the $Cl^- + CH_3I \rightarrow CH_3Cl + I^-$ Potential Energy Surface. *J. Phys. Chem. A* **2009**, *113*, 1976–1984.

- (28) Raghavachari, K.; Trucks, G. W.; Pople, J. A.; Head-Gordon, M. A Fifth-Order Perturbation Comparison of Electron Correlation Theories. *Chem. Phys. Lett.* **1989**, *157*, 479–483.
- (29) Adler, T. B.; Knizia, G.; Werner, H.-J. A Simple and Efficient CCSD(T)-F12 Approximation. *J. Chem. Phys.* **2007**, *127*, 221106.
- (30) Dunning, T. H., Jr. Gaussian Basis Sets for Use in Correlated Molecular Calculations. I. The Atoms Boron Through Neon and Hydrogen. *J. Chem. Phys.* **1989**, *90*, 1007–1023.
- (31) Peterson, K. A.; Figgen, D.; Goll, E.; Stoll, H.; Dolg, M. Systematically Convergent Basis Sets with Relativistic Pseudopotentials. II. Small-Core Pseudopotentials and Correlation Consistent Basis Sets for the Post-*d* Group 16–18 Elements. *J. Chem. Phys.* **2003**, *119*, 11113–11123.
- (32) Peterson, K. A.; Dunning, T. H., Jr. Accurate Correlation Consistent Basis Sets for Molecular Core–Valence Correlation Effects: The Second Row Atoms Al–Ar, and the First Row Atoms B–Ne Revisited. *J. Chem. Phys.* **2002**, *117*, 10548–10560.
- (33) Peterson, K. A.; Yousaf, K. E. Molecular Core-Valence Correlation Effects Involving the Post-*d* Elements Ga–Rn: Benchmarks and New Pseudopotential-Based Correlation Consistent Basis Sets. *J. Chem. Phys.* **2010**, *133*, 174116.
- (34) Allen, W. D.; East, A. L. L.; Császár, A. G. In *Structures and Conformations of Non-Rigid Molecules*; Laane, J., Dakkouri, M., van der Veken, B., Oberhammer, H., Eds.; Kluwer: Dordrecht, 1993; p 343.
- (35) Császár, A. G.; Allen, W. D.; Schaefer, H. F. In Pursuit of the Ab Initio Limit for Conformational Energy Prototypes. *J. Chem. Phys.* **1998**, *108*, 9751–9764.
- (36) Hehre, W. J.; Radom, L.; Schleyer, P. v. R.; Pople, J. A. *Molecular Orbital Theory*; Wiley: New York, 1986.
- (37) Møller, C.; Plesset, M. S. Note on an Approximation Treatment for Many-Electron Systems. *Phys. Rev.* **1934**, *46*, 618–622.
- (38) Purvis, G. D., III; Bartlett, R. J. A Full Coupled-Cluster Singles and Doubles Model: The Inclusion of Disconnected Triples. *J. Chem. Phys.* **1982**, *76*, 1910–1918.
- (39) Noga, J.; Bartlett, R. J. The Full CCSDT Model for Molecular Electronic Structure. *J. Chem. Phys.* **1987**, *86*, 7041–7050.
- (40) Kállay, M.; Gauss, J. Approximate Treatment of Higher Excitations in Coupled-Cluster Theory. *J. Chem. Phys.* **2005**, *123*, 214105.
- (41) Karton, A.; Martin, J. M. L. Comment on: “Estimating the Hartree–Fock Limit from Finite Basis Set Calculations” [Jensen F (2005) *Theor Chem Acc* 113:267]. *Theor. Chem. Acc.* **2006**, *115*, 330–333.
- (42) Klopper, W.; Kutzelnigg, W. Gaussian Basis Sets and the Nuclear Cusp Problem. *J. Mol. Struct.: THEOCHEM* **1986**, *135*, 339–356.
- (43) Tasi, G.; Császár, A. G. Hartree–Fock-Limit Energies and Structures with a Few Dozen Distributed Gaussians. *Chem. Phys. Lett.* **2007**, *438*, 139–143.
- (44) Helgaker, T.; Klopper, W.; Koch, H.; Noga, J. Basis-Set Convergence of Correlated Calculations on Water. *J. Chem. Phys.* **1997**, *106*, 9639–9646.
- (45) Werner, H.-J.; Knowles, P. J.; Knizia, G.; Manby, F. R.; Schütz, M.; et al. MOLPRO, version 2015.1, a package of ab initio programs. <http://www.molpro.net>.
- (46) MRCC, a quantum chemical program suite written by Kállay, M.; Rolik, Z.; Ladjángszki, I.; Szegedy, L.; Ladóczki, B.; Csontos, J.; Kornis, B.; Rolik, Z.; Kállay, M. A General-Order Local Coupled-Cluster Method Based on the Cluster-in-Molecule Approach. *J. Chem. Phys.* **2011**, *135*, 104111 as well as: www.mrcc.hu.
- (47) Xie, J.; McClellan, M.; Sun, R.; Kohale, S. C.; Govind, N.; Hase, W. L. Direct Dynamics Simulation of Dissociation of the [CH₃–I–OH][−] Ion–Molecule Complex. *J. Phys. Chem. A* **2015**, *119*, 817–825.
- (48) Furtenbacher, T.; Czakó, G.; Sutcliffe, B. T.; Császár, A. G.; Szalay, V. The Methylene Saga Continues: Stretching Fundamentals and Zero-Point Energy of X³B₁ CH₂. *J. Mol. Struct.* **2006**, *780*–781, 283–294.
- (49) Czakó, G.; Szabó, I.; Telekes, H. On the Choice of the ab Initio Level of Theory for Potential Energy Surface Developments. *J. Phys. Chem. A* **2014**, *118*, 646–654.
- (50) Ruscic, B.; Pinzon, R. E.; Morton, M. L.; von Laszewski, G.; Bittner, S.; Nijssure, S. G.; Amin, K. A.; Minkoff, M.; Wagner, A. F. Introduction to Active Thermochemical Tables: Several “Key” Enthalpies of Formation Revisited. *J. Phys. Chem. A* **2004**, *108*, 9979–9997.
- (51) Ruscic, B.; Bross, D. H. Active Thermochemical Tables (ATcT) Values Based on Ver. 1.122 of the Thermochemical Network (2016). ATcT.anl.gov.
- (52) Ruscic, B. Active Thermochemical Tables (ATcT) Values Based on Ver. 1.118 of the Thermochemical Network (2015). ATcT.anl.gov.